American Society of Hematology
2021 L Street NW, Suite 900,
Washington, DC 20036
Phone: 202-776-0544 | Fax 202-776-0545
editorial@hematology.org

The ATF4-RPS19BP1 axis modulates ribosome biogenesis to promote erythropoiesis

Tracking no: BLD-2023-021901R1

Zhaofeng Zheng (State Key Laboratory of Experimental Hematology, Institute of Hematology & Blood Diseases Hospital, Chinese Academy of Medical Sciences & Peking Union Medical College; Center for Stem Cell Medicine, Chinese Academy of Medical Sciences; Department of Stem Cell & Regenerative Medicine, Peking Union Medical College, Tianjin, China, China) Shangda Yang (State Key Laboratory of Experimental Hematology, Institute of Hematology & Blood Diseases Hospital, Chinese Academy of Medical Sciences & Peking Union Medical College; Center for Stem Cell Medicine,, China) Fanglin Gou (Department of Cell Biology, School of Basic Medical Sciences, Tianjin Medical University, Tianjin, China, China) Chao Tang (State Key Laboratory of Experimental Hematology, Institute of Hematology and Blood Diseases Hospital, China) Zhaoru Zhang (Zhejiang University, China) Quan Gu (State Key Laboratory of Experimental Hematology, National Clinical Research Center for Blood Diseases, Haihe Laboratory of Cell Ecosystem, Institute of Hematology & Blood Diseases Hospital, Chinese Academy of Medical Sciences & Peking Union Medical College, Tianjin, China, China) Guohuan Sun (State Key Laboratory of Experimental Hematology, Institute of Hematology & Blood Diseases Hospital, Chinese Academy of Medical Sciences & Peking Union Medical College; Center for Stem Cell Medicine,, China) Penglei Jiang (Institute of Hematology, Zhejiang University, China) Nini Wang (State Key Laboratory of Experimental Hematology, Institute of Hematology & Blood Diseases Hospital, Chinese Academy of Medical Sciences & Peking Union Medical College; Center for Stem Cell Medicine, Chinese Academy of Medical Sciences; Department of Stem Cell & Regenerative Medicine, Peking Union Medical College, Tianjin, China, China) Xiangnan Zhao (State Key Laboratory of Experimental Hematology, Institute of Hematology & Blood Diseases Hospital, Chinese Academy of Medical Sciences & Peking Union Medical College; Center for Stem Cell Medicine,, China) Junnan Kang (Tianjin Medical University, China) Yifei Wang (State Key Laboratory of Experimental Hematology, Institute of Hematology & Blood Diseases Hospital, Chinese Academy of Medical Sciences & Peking Union Medical College; Center for Stem Cell Medicine, China) Yicheng He (Institute of Hematology, China) Meng Yang (Institute of Hematology, China) Ting Lu (Institute of Hematology, China) Shihong Lu (State Key Laboratory of Experimental Hematology, Institute of Hematology & Blood Diseases Hospital, Chinese Academy of Medical Sciences & Peking Union Medical College, Tianjin, China, China) Pengxu Qian (Zhejiang University School of Medicine, China) Ping Zhu (State Key Laboratory of Experimental Hematology, Institute of Hematology and Blood Diseases Hospital, China) Hui Cheng (State Key Laboratory of Experimental Hematology, Institute of Hematology & Blood Diseases Hospital, Chinese Academy of Medical Sciences & Peking Union Medical College; Center for Stem Cell Medicine,, China) Tao Cheng (State Key Laboratory of Experimental Hematology, National Clinical Research Center for Blood Diseases, Institute of Hematology & Blood Diseases Hospital, Chinese Academy of Medical Sciences & Peking, China)

Abstract:
Hematopoietic differentiation is controlled by intrinsic regulators and the extrinsic hematopoietic niche. Activating transcription factor 4 (ATF4) plays a crucial role in the function of fetal and adult hematopoietic stem cell maintenance; however, the precise function of ATF4 in the bone marrow niche and the mechanism by which ATF4 regulates adult hematopoiesis remain largely unknown. Here, we employ four cell-type-specific mouse Cre lines to achieve conditional knockout of Atf4 in Cdh5+ endothelial cells, Prx1+ bone marrow stromal cells, Osx+ osteo-progenitor cells, and Mx1+ hematopoietic cells, and uncover the role of Atf4 in niche cells and hematopoiesis. Intriguingly, depletion of Atf4 in niche cells does not affect hematopoiesis; however, Atf4-deficient hematopoietic cells exhibit erythroid differentiation defects, leading to hypoplastic anemia. Mechanistically, ATF4 mediates direct regulation of Rps19bp1 transcription, which is, in turn, involved in 40S ribosomal subunit assembly to coordinate ribosome biogenesis and promote erythropoiesis. Finally, we demonstrate that under conditions of 5-fluorouracil-induced stress, Atf4 depletion impedes the recovery of hematopoietic lineages, which requires efficient ribosome biogenesis. Taken together, our findings highlight the indispensable role of the ATF4-RPS19BP1 axis in the regulation of erythropoiesis.-

Conflict of interest: No COI declared

COI notes:

Preprint server: No;

Author contributions and disclosures: ZF.Z., SD.Y, FL.G., C.T., and ZR.Z. designed the study. Q.G., GH.S., PL.J., NN.W., XN.Z., JN.K., YF.W., YC.H., M.Y., and SH.L. helped with mouse experiments. T.L. helped with bioinformatics analysis. PX.Q., P.Z., H.C. and T.C. proposed the study, designed the experiments, interpreted the results, wrote the paper and oversaw the research project.

Non-author contributions and disclosures: No;

Agreement to Share Publication-Related Data and Data Sharing Statement: RNA-seq and scRNA-seq data have been deposited in the GEO (accession codes GSE233677 and GSE235798, respectively). ATAC-seq and H3K4me3 CUT&Tag data have been deposited in the SRA (accession codes PRJNA992183 and PRJNA992885, respectively). All other data are available from the corresponding authors upon reasonable request. The computational code used in this study can be obtained from P.Z. (zhuping@ihcams.ac.cn).

Clinical trial registration information (if any):

The ATF4-RPS19BP1 axis modulates ribosome biogenesis to promote erythropoiesis

Zhaofeng Zheng[1,2#], Shangda Yang[1,3#], Fanglin Gou[4#], Chao Tang[1,3#], Zhaoru Zhang[5#], Quan Gu[1,3], Guohuan Sun[1,3], Penglei Jiang[5], Nini Wang[1,3], Xiangnan Zhao[1,3,] Junnan Kang[6], Yifei Wang[1,3], Yicheng He[1,3], Meng Yang[1,3], Ting Lu[1,3], Shihong Lu[1,3], Pengxu Qian[5*], Ping Zhu[1,3*], Hui Cheng[1,3*], Tao Cheng[1,3*]

[1]State Key Laboratory of Experimental Hematology, National Clinical Research Center for Blood Diseases, Haihe Laboratory of Cell Ecosystem, Institute of Hematology & Blood Diseases Hospital, Chinese Academy of Medical Sciences & Peking Union Medical College, Tianjin, China

[2]Fujian Institute of Hematology, Fujian Provincial Key Laboratory on Hematology, Fujian Medical University Union Hospital

[3]CAMS Center for Stem Cell Medicine, PUMC Department of Stem Cell and Regenerative Medicine, Tianjin, China

[4]The Province and Ministry Co-sponsored Collaborative Innovation Center for Medical Epigenetics, Key Laboratory of Immune Microenvironment and Disease (Ministry of Education), Department of Cell Biology, Tianjin Medical University, Tianjin, China

[5]Center for Stem Cell and Regenerative Medicine and Bone Marrow Transplantation Center of the First Affiliated Hospital, Zhejiang University School of Medicine; Liangzhu Laboratory, Zhejiang University Medical Center; Institute of Hematology, Zhejiang University; Zhejiang Engineering Laboratory for Stem Cell and Immunotherapy, Hangzhou 310058, China

[6]Department of Hematology, Tianjin Medical University Cancer Institute and Hospital, National Clinical Research Center for Cancer, Key Laboratory of Cancer Prevention and Therapy, Tianjin's Clinical Research Center for Cancer, Tianjin, China

#These authors contributed equally

*Correspondence: chengtao@ihcams.ac.cn (T.C.), chenghui@ihcams.ac.cn (H.C.), zhuping@ihcams.ac.cn (P.Z.), axu@zju.edu.cn (P.Q.)

Data availability

RNA-seq and scRNA-seq data have been deposited in the GEO (accession codes GSE233677 and GSE235798, respectively). ATAC-seq and H3K4me3 CUT&Tag data have been deposited in the SRA (accession codes PRJNA992183 and PRJNA992885, respectively). All other data are available from the corresponding authors upon reasonable request. The computational code used in this study can be obtained from P.Z. (zhuping@ihcams.ac.cn).

Abstract

Hematopoietic differentiation is controlled by intrinsic regulators and the extrinsic hematopoietic niche. Activating transcription factor 4 (ATF4) plays a crucial role in the function of fetal and adult hematopoietic stem cell maintenance; however, the precise function of ATF4 in the bone marrow niche and the mechanism by which ATF4 regulates adult hematopoiesis remain largely unknown. Here, we employ four cell-type-specific mouse Cre lines to achieve conditional knockout of *Atf4* in Cdh5^{+} endothelial cells, Prx1^{+} bone marrow stromal cells, Osx^{+} osteo-progenitor cells, and Mx1^{+} hematopoietic cells, and uncover the role of *Atf4* in niche cells and hematopoiesis. Intriguingly, depletion of *Atf4* in niche cells does not affect hematopoiesis; however, *Atf4*-deficient hematopoietic cells exhibit erythroid differentiation defects, leading to hypoplastic anemia. Mechanistically, ATF4 mediates direct regulation of *Rps19bp1* transcription, which is, in turn, involved in 40S ribosomal subunit assembly to coordinate ribosome biogenesis and promote erythropoiesis. Finally, we demonstrate that under conditions of 5-fluorouracil-induced stress, *Atf4* depletion impedes the recovery of hematopoietic lineages, which requires efficient ribosome biogenesis. Taken together, our findings highlight the indispensable role of the ATF4-RPS19BP1 axis in the regulation of erythropoiesis.

Key Points

- Atf4-deficient hematopoietic cells exhibited HSC function and erythroid differentiation defects.
- ATF4 directly regulates the transcription of Rps19bp1 to coordinate ribosome biogenesis and promote erythropoiesis.

Introduction

The production of mature blood and immune cells is maintained by a rare population of hematopoietic stem cells (HSCs) located in the bone marrow (BM)[1]. HSC function and hematopoiesis are governed by the complex interplay of extrinsic signals from the microenvironment and intrinsic programs encompassing transcription factors (TFs), non-coding RNAs (ncRNAs), and epigenetic modifications[2,3]. Furthermore, the HSC niche formed by various populations such as mesenchymal stromal cells (MSCs), endothelial cells (ECs), and osteoblasts provides the crucial signals and interactions that directly regulate HSC functions[4-9]. Dysregulation of this process can lead to severe hematopoietic failure and/or hematologic malignancies.

Erythropoiesis encompasses two primary phases. In the early phase, HSCs differentiate to generate erythroid progenitors[10]. This is followed erythroid terminal differentiation (ETD), involving a series of morphological and biochemical changes in erythroblasts that culminate in the production of functional red blood cells (RBCs). Critical TFs and other regulatory factors contribute collaboratively to this process[11-16]. Investigations of the signals and regulatory networks governing erythropoiesis are required to elucidate the biology of erythroid cells and identify potential therapeutic approaches to erythroid-related disorders.

ATF4 is induced by signals such as endoplasmic reticulum stress and oxidative stress[17]. Studies in the *Atf4*-knockout mouse model have demonstrated that ATF4 plays a pivotal role in multiple biological processes, including fetal liver hematopoiesis, HSC maintenance, bone formation, and tumorigenesis[18-22]. ATF4 depletion induced partial perinatal lethality and impaired hematopoiesis in the fetal liver, resulting in severe anemia and abnormal erythropoiesis in E15.5 mouse embryos[22]. We previously showed that ATF4 functions in a cell-extrinsic manner to mediate HSC expansion and maintenance in the murine fetal liver by upregulating Angptl3 in niche cells[18]. Sun et al. also reported the role of ATF4 in the regulation of adult HSC aging[20]. Atf4 has also been shown to regulate erythropoiesis via the HRI-eIF2aP-ATF4

axis[23]. This signaling pathway is essential for terminal erythropoiesis under conditions such as iron/heme deficiency, environmental stresses (e.g., oxidative stress), and in the pathological conditions of β-thalassemia[24-26]. ATF4 is highly expressed in proerythroblasts and basophilic erythroblasts (BasoE)[27]. During iron deficiency, ATF4-target genes are highly activated to maintain mitochondrial function, redox homeostasis, and facilitate erythroid differentiation[24]. Additionally, the HRI-eIF2aP-ATF4 axis is involved in control of the expression of gamma-globin and fetal globin through regulation of MYB or BCL11A[28,29]. These observations highlight the pleiotropic role of ATF4 in stress-induced erythropoiesis. Intriguingly, Atf4$^{-/-}$ embryos also develop transient fetal anemia even under iron sufficiency, suggesting a potential role in erythroid development[18]. Thus, in the present study, we investigated whether ATF4 regulates adult HSC function and erythropoiesis at steady-state as well as the underlying mechanisms.

Methods

Mice

Atf4$^{fl/fl}$ mice were generated by Nanjing Biomedical Research Institute of Nanjing University, China. *Cdh5*-CreER mice were generated by Biocytogen Co. Ltd (Beijing, China). C57BL/6, B6.SJL, Col2.3-GFP and β-actin-GFP mice (aged 6–8 weeks) were maintained in the animal facility of the State Key Laboratory of Experimental Hematology (SKLEH; Tianjin, China). All animal experiment protocols were approved by the Institutional Animal Care and Use Committees of SKLEH.

Colony formation assay

Murine BM cells or sorted Lin$^-$cKit$^+$Sca-1$^+$ (LKS$^+$) cells were cultured in M3434 medium (StemCell Technologies) for 7–10 days to generate BFU-E, CFU-G, CFU-M, CFU-GM, and CFU-GEMM colonies. Murine BM, cKit$^+$ or MEP cells were cultured in M3334 medium (StemCell Technologies) for 48 h to generate CFU-E colonies or in M3436 medium (StemCell Technologies) for 10–14 days to generate BFU-E colonies.

BM transplantation

Competitive BM transplantation assay

BM cells (1.5×10^6) from conditional knockout or wild-type (WT) mice (aged 8 weeks) were transplanted with $CD45.1^+$ competitive BM cells (1×10^6) into lethally irradiated $CD45.1^+$ recipients.

Secondary transplantation experiment

BM cells (1.5×10^6) from primary recipients were transplanted into lethally irradiated $CD45.1^+$ recipients.

Reciprocal transplantation experiment

$CD45.1^+$ BM cells (1×10^6) were transplanted into $CD45.2^+$ conditional knockout or wild-type mice.

In each experiment, peripheral blood (PB) reconstitution was monitored every 4 weeks.

Statistical analysis

All data were presented as means obtained from three independent biological experiments ± standard deviation (SD). Two groups were compared with an unpaired, two-tailed Student's *t*-test. Multiple groups were compared with ANOVA with Bonferroni's correction. *P*-values < 0.05 were considered to indicate statistical significance. All statistical analyses and graphs were generated using GraphPad Prism v8.0 software.

The protocols used for the animal experiments were approved by the Institutional Animal Care and Use Committees of SKLEH

Additional methods are provided in the supplemental methods.

Results

ATF4 depletion in MSCs does not affect hematopoiesis

To investigate whether depletion of *Atf4* in niche cells affects hematopoiesis, we crossed Atf4$^{fl/fl}$ mice (fl/fl) with Prx1-Cre mice[30] **(Figure S1A)**. *Atf4* knockout efficiency (95%) was validated by quantitative real-time (qRT)-PCR **(Figure 1A)**. The Prx1-Cre;Atf4$^{fl/fl}$ mice had shortened limbs and reduced body size **(Figure 1B)**. Micro-computed tomography (CT) confirmed the limb defects and revealed a lower trabecular bone number, volume, and mineral density in Prx1-Cre;Atf4$^{fl/fl}$ mice **(Figures 1C–E and S1B)**. The bone formation rate was also reduced following *Atf4* deletion in MSCs **(Figure 1F)**. The results were further confirmed in Prx1-Cre;Atf4$^{fl/fl}$;Col2.3-GFP mice **(Figure 1G)**. Moreover, *Atf4* deletion reduced BM MSC numbers **(Figure 1H)** and impaired their CFU-F activity **(Figure 1I)** as well as differentiation toward osteoblasts and adipocytes **(Figure 1J and S1C)**. These findings indicate that ATF4 is required for MSC function and differentiation.

We next explored the effects of MSC dysfunction induced by *Atf4* depletion on BM hematopoiesis. Compared with littermate controls, Prx1-Cre;Atf4$^{fl/fl}$ mice had half the number of whole BM cells **(Figure 1K)**, while the frequencies of hematopoietic stem and progenitor cells (HSPCs) and lineage cells were similar **(Figure 1L and S1D-E)**. Prx1-Cre;Atf4$^{fl/fl}$ mice also had normal blood cell counts **(Figure S1F)**. BM cells from the two groups yielded comparable numbers of colonies **(Figure 1M)** and competitive BM transplantation assays showed that the repopulation ability, lineage regeneration, and HSC output were similar **(Figure 1N–P and S1G-K)**. MSC-specific *Atf4* deletion affected neither HSC self-renewal in secondary transplantation assays **(Figure 1Q–R**) nor hematopoietic reconstitution, lineage regeneration, and HSC output in reciprocal transplantation **(Figure 1S–U and S1L-M**). Moreover, Prx1-Cre;Atf4$^{fl/fl}$ mice had normal hematopoiesis under 5-fluoruracil (5-FU)-stress (**Figure S1N-R**). These findings indicate that *Atf4* loss in MSCs spares hematopoiesis and HSC function in adult mice.

ATF4 depletion in ECs and osteo-progenitors does not affect

hematopoiesis

To test whether *Atf4* deletion in ECs and osteo-progenitors impacts the adult BM niche and hematopoiesis, we generated Cdh5-CreER;Atf4$^{fl/fl}$ and Osx-CreER;Atf4$^{fl/fl}$ mice, respectively. *Atf4* deletion did not affect the frequency of the relevant niche cells (**Figure S2A–B**). Moreover, the conditional knockout mice had normal blood cell counts **(Figure S2C–D),** BM HSPC frequencies (**Figure S2E–F**), and BM cell colony-forming abilities (**Figure S2G–H**). BM cells from conditional knockout mice and control mice also had similar levels of long-term multilineage reconstitution in competitive reconstitution assays (**Figure 1V–W and S2I–J**). These results indicate that, unlike in the fetal liver, *Atf4* depletion in the MSCs, ECs, or osteo-progenitors of adult mice has a minor effect on BM hematopoiesis and HSC maintenance.

ATF4 depletion from hematopoietic cells impairs HSC self-renewal

To investigate whether ATF4 regulates adult murine hematopoiesis and HSC function in a cell-intrinsic manner, we generated Mx1-Cre;Atf4$^{fl/fl}$ (Δ/Δ) mice. *Atf4* deletion was induced by polyinosinic-polycytidylic acid (pIpC) treatment and mice were sacrificed 1 month later **(Figure 2A and 2B)**. Although there was no difference in the number of total nucleated BM cells between the two groups **(Figure 2C)**, the frequencies of most HSPC subsets (including long-term HSC [LT-HSC], short-term HSC [ST-HSC], multi-potent progenitor [MPP], common myeloid progenitor [CMP], granulocyte-monocyte progenitor [GMP] and PreGM subsets) were increased, whereas those of erythroid progenitor cells (EPCs, including megakaryocyte-erythroid progenitor [MEP], PreCFU-E, and CFU-E cells) were decreased in Δ/Δ mice **(Figure 2D–G and S3A)**. Furthermore, *Atf4* deficiency skewed differentiation toward the myeloid lineage, which was evidenced by a reduction in T and B cell proportions (**Figure 2H**).

We evaluated the impact of ATF4 deficiency on HSC function *in vivo* using competitive BM transplantation assays **(Figure 2I)**. *Atf4* depletion severely impaired the BM repopulation ability **(Figure 2J–K)**. Furthermore, the frequencies of donor-derived MPPs, GMPs, and PreGM subsets were

significantly higher in *Atf4*-deleted donor cells, while those of EPCs (including PreCFU-E and CFU-E) were lower, which was consistent with the phenotype observed at steady-state **(Figure 2L–M)**. Secondary BM transplantation experiments further confirmed that *Atf4* deletion inhibited HSC self-renewal capacity **(Figure 2N)**. To verify that cell-specific *Atf4* deletion led to HSC dysfunction, we performed transplantation assays in which BM cells from Δ/Δ and fl/fl mice were co-transplanted with competitor BM cells into lethally irradiated recipients. pIpC-induced *Atf4* deletion **(Figure S3B)** rapidly reduced the donor-derived cell repopulation ability and increased the frequency of most donor-derived HSPC subsets, while decreasing EPC numbers **(Figure S3C–F)**. These data confirmed that *Atf4* deletion severely impaired HSC self-renewal ability. *In vitro* colony formation assays to evaluate the function of HSPCs showed that LKS^+ cells, whole BM cells and LT-HSCs from the *Atf4*-depleted group formed only a few scattered colonies **(Figure 2O and S3G-H)**. These results demonstrate that *Atf4* deletion leads to HSC functional defects.

ATF4 depletion in hematopoietic cells causes severe macrocytosis

Atf4 loss not only impaired the function of adult HSCs, but also led to a significant decrease in EPC numbers compared with control mice (**Figure 2D–G, 2L and S3F**). In addition, Δ/Δ mice had severe anemia, with fewer RBCs and lower hemoglobin levels **(Figure 3A–B**). The mean corpuscular volume was increased following *Atf4* deletion, suggesting that *Atf4*-deficient mice developed macrocytosis **(Figure 3B**). Crucially, >70% of the Δ/Δ mice died from anemia **(Figure 3C**). These findings show that *Atf4* loss in the hematopoietic cells of adult mice represses erythropoiesis.

To investigate how ATF4 is involved in terminal erythroid differentiation, we characterized the stages of erythropoiesis in the BM by flow cytometry. *Atf4* deletion markedly impaired each stage of terminal erythroid differentiation **(Figure 3D)**. In both groups, the Pro, Baso, Poly, and Ortho erythroblasts within the nucleated erythroblast population were present at a ratio of 1:2:4:8 **(Figure 3E)**. This finding suggests that the blockade of erythroid differentiation

induced by *Atf4* deletion occurred at the progenitor stage.

We next performed *in vitro* erythroid colony formation assays (CFU-E and BFU-E) to evaluate the function of EPCs. cKit$^+$ cells from Δ/Δ mice generated fewer and smaller colonies **(Figure 3F–G)**. In addition, fewer *Atf4*-depleted MEPs entered the cell-cycle compared with WT MEPs **(Figure 3H–I)**. Similarly, MEPs from Δ/Δ mice also generated fewer erythroid colonies (**Figure 3J-K**). We also observed extramedullary hematopoiesis and blocked erythroid commitment in the spleen of Δ/Δ mice **(Figure S4)**. These data suggest that erythroid commitment is blocked by *Atf4* loss.

ATF4 loss alters lineage commitment in HSPCs

To decipher the effect of ATF4 on the transcriptional profiles of HSPC subsets, we performed single-cell RNA sequencing (scRNA-seq) of FACS-sorted BM Lin$^-$cKit$^+$ (LK$^+$) cells from Δ/Δ and fl/fl mice 4 weeks post-*Atf4*-deletion **(Figure 4A)**. We also enriched LK$^+$ cells from the BM of secondary recipient mice for additional scRNA-seq **(Figure S5A–B)**. Uniform manifold approximation and projection (UMAP) analysis and feature gene expression identified 15 distinct clusters **(Figure 4B and S5C; Table S1)**. In accordance with the flow cytometry analysis **(Figure 2E–G),** the frequencies of transcriptomically defined EPCs (including Ery1 and Ery2 subsets) were markedly lower in Δ/Δ mice than in controls, confirming the impairment of erythropoiesis **(Figure 4C–D)**. However, *Atf4* deletion increased the numbers of other HSPC subsets, revealing a shift in transcriptional priming during hematopoiesis **(Figure 4C–D)**. Transcriptional analysis of EPCs in *Atf4*-deficient cells further supported the impaired terminal maturation of these cells **(Figure 4E)**. FateID analysis showed that *Atf4*-depleted HSC/MPPs exhibited reduced differentiation into the erythroid lineage, suggesting that transcriptional priming had already occurred in HSC/MPPs **(Figure 4F and S5D)**. The post-transplant Δ/Δ mice also had lower numbers of transcriptomically detected Ery1 and Ery2 subsets **(Figure S5E-F)**.

CMPs lie upstream of MEPs and their lineage output is highly heterogeneous[31].

We then performed scRNA-seq of flow-cytometry-sorted CMP cells from Δ/Δ and fl/fl mice. Clustering analysis generated a map with eight transcriptional subpopulations **(Figure 4G and S5G-I; Table S2)**. In the Δ/Δ group, the sizes of the erythroid (E) groups were significantly reduced **(Figure 4H–I)**. These results suggest that *Aft4* deletion biased the lineage output of CMPs and impaired erythroid differentiation.

ATF4 deletion forces early erythroid progenitors into S phase

To elucidate the mechanism of impaired erythropoiesis in Δ/Δ mice, we examined transcriptomically detected Ery1 and Ery2 cells at steady-state. Cell-cycle analysis revealed a higher proportion of Ery1 cells from the Δ/Δ group in the S and G2/M phases **(Figure 4J)**. Similarly, the expression of genes associated with the G1/S transition was significantly increased in Ery1 cells from Δ/Δ mice **(Figure 4K and S6A)**. Conversely and in accordance with the changes observed in flow-defined MEP cells, fewer Ery2 cells from the Δ/Δ group were in the S and G2/M phases **(Figure 4J and 3H–I)**. DNA replication was hyperactivated in Ery1 cells from Δ/Δ mice **(Figure 4L–N)**, which induced the Ery1 cells response to replication stress **(Figure 4O–P and S6B)**. Furthermore, the DNA damage response and DNA repair pathway were induced in *Atf4*-depleted Ery1 cells **(Figure 4Q–R and S6C–D)**. Consequently, apoptosis-related gene (e.g., *Bax*) expression was elevated **(Figure 4S–T and S6E)**.

We explored the existence of this phenomenon in CMPs by cell-cycle analysis of erythroid clusters in Δ/Δ and fl/fl mice. A greater number of E cells from the Δ/Δ group were in S phase, as evidenced by the increased expression of G1/S transition-related genes **(Figure S6F-G)**. In line with the changes in Ery1 cells, *Atf4*-deleted E cells displayed higher levels of DNA replication and subsequent replication stress, which induced DNA damage, DNA repair, and apoptosis **(Figure S6H-L)**. These transcriptomic changes were validated by computational screening for surface markers over-represented in the E clusters and isolating E clusters with an immunophenotype of $Lin^{-}cKit^{+}Sca1^{-}CD34^{+}CD16/32^{low}CD55^{+}CD63^{-}CD41^{-}$ from BM (**Figure S6M-O**)

for *in vitro* experiments (**Figure S6P-R**). These results suggest that the absence of ATF4 forced erythroid progenitors into the S phase, leading to replication stress and activation of both the DNA damage response and apoptosis.

ATF4 directs the transcriptional program of erythropoiesis

To investigate the molecular mechanism by which *Atf4* deficiency causes severe impairment of erythropoiesis, we sorted MEPs from Δ/Δ and fl/fl mice 4 weeks post-*Atf4* deletion for RNA-seq **(Figure 5A)**. In total, we identified 4,704 differentially expressed genes (DEGs) between the Δ/Δ and fl/fl groups, of which, 897 were downregulated **(Figure 5B)**. Gene ontology (GO) analysis of downregulated genes revealed impaired erythrocyte development in Δ/Δ mice **(Figure 5C)**, which was consistent with the colony formation assay results **(Figure 3J-K)**. In addition, we performed transposase-accessible chromatin (ATAC)-seq with MEP cells to explore the changes in chromatin accessibility following *Atf4* deletion **(Figure 5A, 5D–E)**. We identified 29,493 different peaks of accessibility between the Δ/Δ and fl/fl mouse groups,17.83% of which were localized to the promoter **(Figure 5F)**.

We also conducted cleavage under targets and tagmentation (CUT&Tag) assays using MEP cells and an antibody against the trimethylation of histone H3 lysine 4 (H3K4me3) histone modification **(Figure 5G)**. Integrative analyses of RNA-seq, ATAC-seq, and H3K4me3 CUT&Tag datasets yielded 81 genes that were downregulated (transcriptionally repressed) in Δ/Δ versus fl/fl mice **(Figure 5H; Table S3)**. GO analysis of these genes revealed that several terms related to erythropoiesis were highly diminished in *Atf4*-deficient MEPs **(Figure 5I)**. qRT-PCR analysis further confirmed the decreased expression of erythrocyte differentiation-related genes **(Figure 5J)**. Visualization of ATAC-seq and H3K4me3 CUT&Tag data showed that the peaks of erythroid master regulators *Klf1* and *Tal1* were decreased in *Atf4*-depleted MEPs **(Figure 5K)**.

Interestingly, the top-ranked downregulated gene sets from bulk RNA-seq data

of *Atf4*-depleted CMPs and LT-HSCs were implicated in erythrocyte development **(Figure S7A–D).** GO analysis of the ATAC-seq and H3K4me3 CUT&Tag datasets showed that 56 overlapping genes were downregulated in *Atf4*-deficient LT-HSCs; these genes were enriched in pathways associated with negative regulation of cell proliferation **(Figure S7E–I)**. These results suggest that the absence of ATF4 impairs erythroid differentiation from HSCs.

ATF4 activates the transcription of *Rps19bp1* to regulate ribosome biogenesis

In subsequent integrative analysis of the genes that were identified as downregulated in MEPs by RNA-seq, ATAC-seq, and H3K4me3 CUT&Tag and genes that were identified as downregulated in erythroid progenitors (i.e., PreMegE, Ery1, and Ery2) by scRNA-seq, we identified two genes, *Car1* and *Rps19bp1* **(Figure 6A)**. Intriguingly, *Rps19bp1* was among the overlapping downregulated genes identified in the RNA-seq analysis of LT-HSCs and HSC/MPPs **(Figure S8A)**. qRT-PCR analysis showed a marked reduction in *Rps19bp1* expression in *Atf4*-deleted MEPs compared with controls **(Figure 6B)**. Analysis of scRNA-seq data using pySCENIC predicted *Rps19bp1* as a target gene of *Atf4* **(Figure 6C)**. scRNA-seq data of CMPs further showed lower *Rps19bp1* expression in *Atf4*-deleted HSPCs, and especially in *Atf4*-deleted erythroid progenitors **(Figure 6D and S8B).**

Luciferase reporter and quantitative chromatin immunoprecipitation (qChIP) assays confirmed that ATF4 regulated *Rps19bp1* transcription **(Figure 6E-F and S8C)** and bound directly to its promoter region **(Figure 6G).** These data indicate that ATF4 is a transcriptional activator of *Rps19bp1*.

Since Rps19bp1 was reported to interact with RPS19 to function in ribosome biogenesis[32], we measured the relative ribosomal protein abundance in ribosomes extracted from *Atf4*-knockdown and WT MEL cells. *Atf4* downregulation decreased the abundance of 40S proteins **(Figure 6H)**. We then administered O-propargyl-puromycin (OP-Puro) to BM HSPCs to assess their translation rates. The MEPs from Δ/Δ mice exhibited markedly lower

levels of fluorescence than those of fl/fl mice **(Figure 6I)**. Moreover, surface sensing of translation (SUnSET) assays confirmed the reduction in the global protein synthesis rate of cKit$^+$ cells from Δ/Δ mice compared with the same cells from fl/fl mice **(Figure 6J–K)**. Transfection of Flag-Rps19bp1 plasmids into *Atf4*-deficient MEL cells or primary cKit$^+$ cells from Δ/Δ mice showed that *Rps19bp1* overexpression reversed the decrease in 40S protein levels **(Figure 6L)**. These results indicate that ATF4 participates in ribosome biogenesis and protein synthesis by regulating *Rps19bp1* transcription.

ATF4 deletion induces Rps19bp1 downregulation and ultimately perturbs erythropoiesis

To investigate the impact of Rps19bp1 on erythroid differentiation in *Atf4*-depleted HSPCs, we transfected Flag-Rps19bp1 plasmids into primary cKit$^+$ cells from Δ/Δ and fl/fl mice and performed *in vitro* CFU-E and BFU-E colony formation assays **(Figure 6J)**. *Rps19bp1* overexpression reversed the decrease in CFU-E and BFU-E colony numbers caused by *Atf4* deletion **(Figure 6M–N and S8D)**. We then transplanted cKit$^+$ cells from Δ/Δ or fl/fl mice transfected with Flag-Rps19bp1-TD, Flag-Rps19bp1-Mut-TD plasmid (introducing an enzyme activity mutation by deleting amino acids 64–73 homologous to human amino acids 62–71)[33] or vector plasmids, together with fresh BM cells from β-actin-GFP transgenic reporter mice, into CD45.1 recipients **(Figure 6O)**. The defective erythropoiesis phenotype of *Atf4*-depleted cells was effectively rescued by overexpression of *Rps19bp1* or the *Rps19bp1* mutant **(Figure 6P and S8F-G)**. Interestingly, *Rps19bp1* overexpression also significantly improved the HSC repopulating ability **(Figure S8H-I)**. In addition, *Rps19bp1* knockdown impaired the repopulation ability and erythrocyte output of cKit$^+$ cells **(Figure S8J-N)**. These findings imply that ATF4 promotes erythroid differentiation and HSC function by boosting *Rps19bp1* transcription, which increases ribosome assembly.

ATF4 depletion accelerates BM hematopoietic failure in response to 5-FU-induced stress

To better understand the consequences of decreased ribosome levels on

translation following *Atf4* deletion, we sorted CMP cells from Δ/Δ and fl/fl mice 4 weeks post-*Atf4* deletion and conducted ribosome profiling (Ribo-seq)[34] **(Figure 7A)**. We identified 249 significantly differentially translated proteins between the *Atf4*-depleted and control groups **(Figure 7B; Table S4)**. Gene set enrichment analysis (GSEA) further demonstrated that ribosome biogenesis-related protein expression was significantly lower in *Atf4*-depleted than in WT CMP cells, despite no change in their mRNA levels **(Figure 7C–D)**. This observation suggests that the perturbation of ribosome homeostasis has a reciprocal impact on the translation of ribosome-related proteins, potentially exacerbating protein synthesis impairment. The expression of gene sets linked to PreCFU-E signature was also lower in *Atf4*-depleted than in WT CMPs, suggesting that the reduction in ribosome biogenesis significantly affected the translation efficiency of erythroid-related pathway components, thereby impeding erythroid lineage commitment **(Figure 7E)**. Additionally, MEPs exhibited the highest levels of translational activity, while those of CMPs and GMPs were considerably lower, demonstrating a preferential requirement for ribosome biogenesis in early EPCs **(Figure 7F)**. Polysome profiling of FACS-sorted BM cKit$^+$ cells from pIpC-induced Δ/Δ and fl/fl mice also showed a reduction in the relative abundance of the 40S subunit, assembled 80S ribosomes, and polysomes in Δ/Δ cKit$^+$ cells **(Figure 7G)**.

Higher levels of protein synthesis are required during HSPC regeneration after 5-FU exposure. Therefore, to further investigate the effect of ATF4 depletion on BM hematopoiesis under conditions of 5-FU stress, we treated Δ/Δ and fl/fl mice with a single dose of 5-FU (150 mg/kg). The survival of Δ/Δ mice was strikingly reduced compared with fl/fl mice **(Figure 7H)**. Moreover, BM cellularity and LT-HSC numbers were substantially lower in Δ/Δ mice **(Figure 7I–J)**. We also observed a drastic reduction in the number of RBCs, WBCs, and platelets in Δ/Δ mice at day 10 post-treatment **(Figure 7K)**. Further analysis of cKit$^+$ cells isolated on day 10 post-treatment using SUnSET showed a more pronounced reduction in protein synthesis levels in Δ/Δ mice even after treatment with 5-FU compared with fl/fl mice **(Figure 7L)**. These results reveal that the absence of ATF4 under stress conditions hinders

hematopoietic lineage development as it relies on robust ribosome biogenesis, and ultimately results in BM failure.

Discussion

Previous studies have indicated that erythroid progenitors have unique cell-cycle signatures, with shorter cell-cycle duration and a faster DNA synthesis rate during the commitment from self-renewal to differentiation[35,36]. Our data showed that MEPs exhibited much higher protein synthesis rates than GMPs or CMPs, suggesting that they are especially sensitive to ribosome biogenesis defects. This may explain the severe perturbation of the erythroid lineage in *Atf4*-depleted mice. Our findings highlight the crucial importance of protein synthesis regulation during erythroid lineage commitment.

RPS19BP1, which is associated with 40S ribosomal subunits[32], has been reported to bind directly to SIRT1. This interaction enhances the ability of SIRT1 to deacetylate multiple transcription factors or co-factors, including p53, HIF-1α, NF-κB, to regulate the transcription of their target genes, which impact multiple biological processes such as cell differentiation, apoptosis, autophagy and metabolism[37]. However, the observation that overexpression of a catalytically inactive form of RPS19BP1 in Atf4-deleted cKit^{+} cells still rescued the erythroid differentiation blockade caused by ATF4 knockout indicates that the ATF4-RPS19BP1 signaling axis might not regulate erythroid differentiation via the SIRT1 pathway.

Although most Atf4 germline knockout mice (Atf4$^{-/-}$) died neonatally[22], the few survivors exhibited phenotypic expansion of most HSPC subsets (including HSCs, MPPs, CMPs and GMPs), myeloid differentiation skewing, defective colony-forming ability, and impaired self-renewal activity of HSCs[20], which is consistent with the phenotype observed in our study using Mx1-Cre;Atf4$^{fl/fl}$ mice. Furthermore, Atf4$^{-/-}$ or Scl-Cre-ERT;Atf4$^{fl/fl}$ mice displayed normal erythropoiesis in the steady-state[20]. In contrast, Mx1-Cre;Atf4$^{fl/fl}$ mice exhibited severe anemia characterized by reduced MEPs, RBCs and lower hemoglobin levels compared to control mice. Under conditions of iron deficiency stress,

Atf4$^{-/-}$ mice displayed microcytic hypochromic anemia, with inhibited erythroid differentiation starting from basophilic erythroblasts or an earlier stage, resulting in reduced erythroblasts and reticulocytes in the spleen and decreased Ter119^{+} cells in the BM[24]. Therefore, using different mouse models, we expanded the understanding of the role of ATF4 in hematopoiesis.

In summary, by using niche or hematopoietic cell-specific conditional knockout mouse models, we demonstrated that, unlike in the fetal liver, ATF4 governs adult HSC function and erythropoiesis in a cell-intrinsic manner. We revealed a novel role for ATF4 in erythropoiesis, which links it to RPS19BP1, ribosome biogenesis and protein translation. Our findings highlight the crucial importance of protein synthesis regulation during erythroid lineage commitment, a discovery that has extended implications for understanding and treating ribosomopathy-associated erythroid failure.

Acknowledgments

We are grateful to our lab. members for their assistance with the experiments. This work was supported by grants from the Ministry of Science and Technology of China (2021YFA1100900, 2020YFE0203000, 2022YFA1103500), the National Natural Science Foundation of China (92368202, 82270120, 82222003, 92268117, 82161138028), the Haihe Laboratory of Cell Ecosystem Innovation Fund (22HHXBSS00016), the CAMS Initiative for Innovative Medicine (2021-I2M-1–019 and 2021-I2M-1–040), the CAMS Fundamental Research Funds for Central Research Institutes (3332021093).

Authorship contributions

ZF.Z., SD.Y, FL.G., C.T., and ZR.Z. designed the study. Q.G., GH.S., PL.J., NN.W., XN.Z., JN.K., YF.W., YC.H., M.Y., and SH.L. helped with mouse experiments. T.L. helped with bioinformatics analysis. PX.Q., P.Z., H.C. and T.C. proposed the study, designed the experiments, interpreted the results, wrote the paper and oversaw the research project.

Disclosure of conflicts of interest

The authors declare no competing interests.

References

1. Cheng H, Zheng Z, Cheng T. New paradigms on hematopoietic stem cell differentiation. *Protein Cell*. 2020;11(1):34-44.
2. Yang S, Sun G, Wu P, et al. WDR82-binding long noncoding RNA lncEry controls mouse erythroid differentiation and maturation. *The Journal of Experimental Medicine*. 2022;219(4).
3. Huang D, Chen C, Xie L, Yu Z, Zheng J. Hematopoietic stem cell metabolism and stemness. *Blood Sci*. 2019;1(1):12-18.
4. Crane GM, Jeffery E, Morrison SJ. Adult haematopoietic stem cell niches. *Nat Rev Immunol*. 2017;17(9):573-590.
5. Kunisaki Y, Bruns I, Scheiermann C, et al. Arteriolar niches maintain haematopoietic stem cell quiescence. *Nature*. 2013;502(7473):637-643.
6. Bruns I, Lucas D, Pinho S, et al. Megakaryocytes regulate hematopoietic stem cell quiescence through CXCL4 secretion. *Nat Med*. 2014;20(11):1315-1320.
7. Itkin T, Gur-Cohen S, Spencer JA, et al. Distinct bone marrow blood vessels differentially regulate haematopoiesis. *Nature*. 2016;532(7599):323-328.
8. Jiang L, Han X, Wang J, et al. SHP-1 regulates hematopoietic stem cell quiescence by coordinating TGF-β signaling. *J Exp Med*. 2018;215(5):1337-1347.
9. Derecka M, Herman JS, Cauchy P, et al. EBF1-deficient bone marrow stroma elicits persistent changes in HSC potential. *Nat Immunol*. 2020.
10. Tusi BK, Wolock SL, Weinreb C, et al. Population snapshots predict early haematopoietic and erythroid hierarchies. *Nature*. 2018;555(7694):54-60.
11. Fujiwara Y, Browne CP, Cunniff K, Goff SC, Orkin SH. Arrested development of embryonic red cell precursors in mouse embryos lacking transcription factor GATA-1. *Proc Natl Acad Sci U S A*. 1996;93(22):12355-12358.
12. Xu J, Shao Z, Glass K, et al. Combinatorial assembly of developmental stage-specific enhancers controls gene expression programs during human erythropoiesis. *Dev Cell*. 2012;23(4):796-811.
13. Mukherjee K, Xue L, Planutis A, Gnanapragasam MN, Chess A, Bieker JJ. EKLF/KLF1 expression defines a unique macrophage subset during mouse erythropoiesis. *Elife*. 2021;10.
14. Hu W, Yuan B, Flygare J, Lodish HF. Long noncoding RNA-mediated anti-apoptotic activity in murine erythroid terminal differentiation. *Genes Dev*. 2011;25(24):2573-2578.
15. Liu J, Li Y, Tong J, et al. Long non-coding RNA-dependent mechanism to regulate heme biosynthesis and erythrocyte development. *Nat Commun*. 2018;9(1):4386.
16. Yang S, Sun G, Wu P, et al. WDR82-binding long noncoding RNA lncEry controls mouse erythroid differentiation and maturation. *J Exp Med*. 2022;219(4).
17. Ameri K, Harris AL. Activating transcription factor 4. *Int J Biochem Cell Biol*. 2008;40(1):14-21.
18. Zhao Y, Zhou J, Liu D, et al. ATF4 plays a pivotal role in the development of functional hematopoietic stem cells in mouse fetal liver. *Blood*. 2015;126(21):2383-2391.
19. Wortel IMN, van der Meer LT, Kilberg MS, van Leeuwen FN. Surviving Stress: Modulation of ATF4-Mediated Stress Responses in Normal and Malignant Cells. *Trends Endocrinol Metab*. 2017;28(11):794-806.
20. Sun Y, Lin X, Liu B, et al. Loss of ATF4 leads to functional aging-like attrition of adult hematopoietic stem cells. *Sci Adv*. 2021;7(52):eabj6877.

21. Yang X, Matsuda K, Bialek P, et al. ATF4 is a substrate of RSK2 and an essential regulator of osteoblast biology; implication for Coffin-Lowry Syndrome. *Cell*. 2004;117(3):387-398.

22. Masuoka HC, Townes TM. Targeted disruption of the activating transcription factor 4 gene results in severe fetal anemia in mice. *Blood*. 2002;99(3):736-745.

23. Chen JJ, Zhang S. Heme-regulated eIF2α kinase in erythropoiesis and hemoglobinopathies. *Blood*. 2019;134(20):1697-1707.

24. Zhang S, Macias-Garcia A, Velazquez J, Paltrinieri E, Kaufman RJ, Chen JJ. HRI coordinates translation by eIF2alphaP and mTORC1 to mitigate ineffective erythropoiesis in mice during iron deficiency. *Blood*. 2018;131(4):450-461.

25. Chen J-J, Zhang S. Heme-regulated eIF2α kinase in erythropoiesis and hemoglobinopathies. *Blood*. 2019;134(20):1697-1707.

26. Han A-P, Fleming MD, Chen J-J. Heme-regulated eIF2alpha kinase modifies the phenotypic severity of murine models of erythropoietic protoporphyria and beta-thalassemia. *The Journal of Clinical Investigation*. 2005;115(6):1562-1570.

27. Chen JJ, Zhang S. Translational control by heme-regulated eIF2alpha kinase during erythropoiesis. *Curr Opin Hematol*. 2022;29(3):103-111.

28. Boontanrart MY, Schroder MS, Stehli GM, et al. ATF4 Regulates MYB to Increase gamma-Globin in Response to Loss of beta-Globin. *Cell Rep*. 2020;32(5):107993.

29. Huang P, Peslak SA, Lan X, et al. The HRI-regulated transcription factor ATF4 activates BCL11A transcription to silence fetal hemoglobin expression. *Blood*. 2020;135(24):2121-2132.

30. Ding L, Morrison SJ. Haematopoietic stem cells and early lymphoid progenitors occupy distinct bone marrow niches. *Nature*. 2013;495(7440):231-235.

31. Paul F, Arkin Y, Giladi A, et al. Transcriptional Heterogeneity and Lineage Commitment in Myeloid Progenitors. *Cell*. 2015;163(7):1663-1677.

32. Knight JRP, Willis AE, Milner J. Active regulator of SIRT1 is required for ribosome biogenesis and function. *Nucleic Acids Research*. 2013;41(7):4185-4197.

33. Weiss S, Adolph RS, Schweimer K, et al. Molecular Mechanism of Sirtuin 1 Modulation by the AROS Protein. *Int J Mol Sci*. 2022;23(21).

34. Gobet C, Naef F. Ribosome profiling and dynamic regulation of translation in mammals. *Curr Opin Genet Dev*. 2017;43:120-127.

35. Pop R, Shearstone JR, Shen Q, et al. A key commitment step in erythropoiesis is synchronized with the cell cycle clock through mutual inhibition between PU.1 and S-phase progression. *PLoS Biol*. 2010;8(9).

36. Wang B, Wang C, Wan Y, et al. Decoding the pathogenesis of Diamond-Blackfan anemia using single-cell RNA-seq. *Cell Discov*. 2022;8(1):41.

37. Yang Y, Liu Y, Wang Y, et al. Regulation of SIRT1 and Its Roles in Inflammation. *Front Immunol*. 2022;13:831168.

Figure legends

Figure 1. *Atf4* deficiency alters MSC function but not HSC maintenance. A. Quantitative qRT-PCR analysis of *Atf4* expression in CD45$^-$Ter119$^-$LepR$^+$ cells from Prx1-Cre;Atf4$^{fl/fl}$ and Atf4$^{fl/fl}$ mice (n = 3 mice). B. Gross phenotype of Atf4$^{fl/fl}$ and Prx1-Cre;Atf4$^{fl/fl}$ mice at 7 weeks of age (left) and body, forelimb, and hindlimb length measurements (right). ***P < 0.001, **P < 0.01, n = 5. C. Micro-CT image showing the limb phenotype of the *Atf4*-mutant versus wild-type mice. D and E. The micro-CT analysis showing the decreased bone volume fraction in *Atf4* mutants; BV/TV = bone volume per total volume (n = 5 mice). F. Representative calcein double-labeling images (left) with quantification of trabecular bone formation in the femur metaphysis (right) (n = 4–6 mice). G. Representative femur sections from Prx1-Cre;Atf4$^{fl/fl}$;Col2.3-GFP and Atf4$^{fl/fl}$;Col2.3-GFP mice showing the decrease in the number of Col2.3-GFP$^+$ osteoblasts (n= 3 mice). H. Representative flow cytometry dot plots of CD45$^-$Ter119$^-$LepR$^+$ cells (left) and corresponding quantitative data showing the decreased frequency of CD45$^-$Ter119$^-$LepR$^+$ cells in Prx1-Cre;Atf4$^{fl/fl}$ mice at 7 weeks of age (right) (n = 3–4 mice). I. Representative images of CFU-F colonies formed when cells were cultured from enzymatically dissociated bone marrow (left) and the corresponding quantitative data (right); n = 3 mice from at least three independent experiments. J. Representative images of CFU-F differentiating into osteoblasts after culture in differentiation medium for 2–3 weeks, showing the reduced osteogenic potential of *Atf4*-depleted MSCs. K. BM cell numbers of Prx1-Cre;Atf4$^{fl/fl}$ and Atf4$^{fl/fl}$ mice (n = 3 mice). L. Percentages of the indicated cell populations in Prx1-Cre;Atf4$^{fl/fl}$ and Atf4$^{fl/fl}$ mice BM (n = 3 mice). M. Results from colony formation assays using 10^4 BM cells cultured for 10–14 days in complete methylcellulose-based medium (n = 3 mice). N. Experimental workflow of competitive transplantation. O. Percentage of CD45.2$^+$ donor cells in the peripheral blood (PB) of recipient mice at the indicated time-points after competitive BM transplantation (n = 4–8 mice). P. Percentage of CD45.2$^+$ donor-derived HSCs in the BM of recipients (n = 5 mice). Q. Percentage of CD45.2$^+$ donor cells in the PB of recipient mice at the indicated time-points after the secondary BM transplantation (n = 4–7 mice). R. Percentage of

CD45.2$^+$ donor-derived HSCs in the BM of recipients after the secondary BM transplantation (n = 4 mice). S. Experimental workflow of the assay in which 10^6 BM cells were transplanted from donor mice (CD45.1) into irradiated Prx1-Cre;Atf4$^{fl/fl}$ or Atf4$^{fl/fl}$ mice. T. Percentage of CD45.1$^+$ donor cells in the PB of recipient mice at the indicated time-points after BM transplantation. The donor cells were CD45.1$^+$ (n = 5 mice). U. Percentage of CD45.1$^+$ donor-derived HSCs in the BM of recipients (n = 4–5 mice). V–W. Percentage of CD45.2$^+$ donor cells in the PB of recipient mice at the indicated time-points after competitive BM transplantation (n = 4–6 mice). Data represent the mean ± SD. *, $P < 0.05$; **, $P < 0.01$; ***, $P < 0.001$; unpaired two-tailed Student's *t*-test.

Figure 2. ATF4 depletion from hematopoietic cells impairs HSC self-renewal

A. Experimental workflow showing that Mx1-Cre;Atf4$^{fl/fl}$ (Δ/Δ) and Atf4$^{fl/fl}$ (fl/fl) mice were given polyinosinic-polycytidylic acid (pIpC) and sacrificed for analysis 1 month later. B. qRT-PCR analysis of *Atf4* expression in BM cells of fl/fl and Δ/Δ mice (n = 4 mice). C. BM cell numbers of fl/fl and Δ/Δ mice (n = 4–5 mice). D-H. Percentages of the indicated cell populations in the BM of fl/fl and Δ/Δ mice (n = 4–5 mice). I. Experimental workflow for serial and competitive transplantation. J. Percentages of CD45.2$^+$ donor cells in the PB of recipient mice at the indicated time-points after competitive BM transplantation (n = 5–8 mice). K. Percentages of CD45.2$^+$ donor-derived cells in the BM of recipients (n= 3–4 mice). L-M. Percentages of different CD45.2$^+$ donor-derived cell populations in the BM of recipients (n= 3–4 mice). N. Percentages of CD45.2$^+$ donor cells in the PB of recipient mice at the indicated time-points after the secondary BM transplantation (n = 7 mice). O. Results from CFU colony assays performed using 150 LKS$^+$ cells from fl/fl and Δ/Δ mice cultured for 10–14 days in complete methylcellulose-based medium (n = 4–5 wells for 3 independent experiments).

Figure 3. Mx1-Cre;Atf4$^{fl/fl}$ mice experience severe macrocytosis.

A. Representative images of femurs and representative peripheral blood

674 smears. B. The routine blood parameters of fl/fl and Δ/Δ mice (n = 4–5 mice).
675 RBC, red blood cell; HGB, hemoglobin; MCV, mean corpuscular volume;
676 MCHC, mean corpuscular hemoglobin concentration. C. Survival curves of fl/fl
677 and Δ/Δ mice treated with 25 μg/g pIpC delivered on alternate days for a total
678 of three doses. D. The percentages of terminal erythroid cell populations in the
679 BM (n = 3–4 mice). E. Representative flow cytometry dot plots of CD44
680 expression versus FSC, after gating on TER119$^+$ cells (left) and quantification
681 of terminally differentiated erythroid subsets in fl/fl and Δ/Δ mice (right) (n = 4–
682 5 mice). F. Quantitative results from BFU-E colony formation assays performed
683 using 3 × 10^3 cKit$^+$ BM cells from fl/fl and Δ/Δ mice cultured in MethoCult™ SF
684 M3436 methylcellulose-based medium for 10–14 days (n = 4 mice). G.
685 Quantitative results (left) from CFU-E colony formation assays performed
686 using 3 × 10^3 cKit$^+$ BM cells from fl/fl and Δ/Δ mice cultured in MethoCult™ SF
687 M3334 methylcellulose-based medium for 48 h and representative images
688 from three independent experiments (right). Scale bar, 25 μm (n = 4 mice). H.
689 Representative flow cytometry dot plots (BrdU/Hoechst) of MEP cells (left) and
690 a graph showing the percentages of BrdU$^+$ MEP cells (right) (n = 3–4 mice). I.
691 Percentages of MEP cells in different cell-cycle phases (n = 3–4 mice). J.
692 Quantitative results (left) from CFU-E colony formation assays performed
693 using 500 fresh BM MEP sorted from fl/fl and Δ/Δ mice and cultured in
694 MethoCult™ SF M3334 methylcellulose-based medium for 48 h (right), (n = 3
695 mice). K. Quantitative results (left) from BFU-E colony formation assays
696 performed using 1,000 fresh BM MEP cells sorted from fl/fl and Δ/Δ mice and
697 cultured in MethoCult™ SF M3436 methylcellulose-based medium for 2 weeks
698 (right), (n = 3 mice). Data represent the mean ± SD. *, $P < 0.05$; **, $P < 0.01$;
699 ***, $P < 0.001$; unpaired two-tailed Student's *t*-test.
700

701 **Figure 4. ATF4 loss alters transcriptional lineage commitment in HSPCs.**
702 A. Experimental workflow showing the strategy used to sort cells from the
703 bone marrow (BM) of fl/fl and Δ/Δ mice (n = 3 mice) for single-cell RNA
704 sequencing (scRNA-seq). B. UMAP visualization of 14,189 BM lineage$^-$cKit$^+$
705 (LK$^+$) cells categorized into 15 clusters from fl/fl and Δ/Δ mice. C. UMAP plot
706 showing the cell subset distribution frequencies within the fl/fl and Δ/Δ BM LK$^+$

cell populations. D. Transcriptome cluster frequency changes in *Atf4*-depleted LK^+ cells relative to the control. **, $P < 0.01$, ***, $P < 0.001$; Chi-squared test. E. UMAP plots colored according to genotype (fl/fl: blue, 1,544 cells; Δ/Δ: red, 117 cells) (left). The fourth principal component, which had the strongest correlation with erythrocyte maturation, was used to construct the erythrocyte maturation score. Each dot represents a single cell. The distribution of cells according to their erythrocyte maturation scores (right). ***, $P < 0.001$; Wilcoxon rank-sum test. F. Barplot showing the fate bias of single HSC/MPPs computed by FateID. **, $P < 0.01$, ***, $P < 0.001$, ns indicates no significance; two-sided Fisher's exact test. G. UMAP visualization of 19,706 CMP cells from fl/fl and Δ/Δ mice categorized into eight clusters. H. UMAP plot showing the cell subset distribution frequencies in the fl/fl and Δ/Δ CMP cell populations. I. Transcriptome cluster frequency changes in *Atf4*-depleted CMP cells relative to the control. *, $P < 0.05$, ***, $P < 0.001$; Chi-squared test. J. Cell-cycle distributions of Ery1 and Ery2 in fl/fl and Δ/Δ LK^+ cells. K. Violin plots showing the expression of the G1/S phase transition gene set in Ery1 and Ery2 cells from fl/fl and Δ/Δ group. L. Violin plots showing the expression level of the DNA replication gene set in Ery1 and Ery2 cells from fl/fl and Δ/Δ groups. ***, $P < 0.001$, ns indicates no significance; Wilcoxon Rank-sum test. M. Gene set enrichment analysis (GSEA) of DNA replication in Ery1 cells from the fl/fl and Δ/Δ groups. N. Expression levels of representative genes related to DNA replication in Ery1 subsets within the fl/fl and Δ/Δ LK^+ cell populations. O. Violin plots showing the expression of the replication stress gene set in Ery1 and Ery2 cells from the fl/fl and Δ/Δ groups. P. GSEA of replication stress in Ery1 cells from the fl/fl and Δ/Δ groups. Q. GSEA of DNA damage in Ery1 cells from the fl/fl and Δ/Δ groups. R. Violin plots showing the expression of the DNA repair gene set in Ery1 and Ery2 cells from the fl/fl and Δ/Δ groups. S. Violin plots showing the expression of the apoptosis gene set in Ery1 and Ery2 from the fl/fl and Δ/Δ groups. T. GSEA of apoptosis in Ery1 cells from the fl/fl and Δ/Δ groups. *, $P < 0.05$, ***, $P < 0.001$, ns indicates no significance; Wilcoxon rank-sum test.

Figure 5. ATF4 governs the transcriptional program of erythropoiesis.

A. Experimental workflow showing the strategy used to sort the indicated cell types from the BM of fl/fl and Δ/Δ mice (n = 8–10 mice) for bulk RNA-seq, ATAC-seq, and CUT&Tag (H3K4me3). B. Plots showing the differentially expressed genes identified from bulk RNA-seq analysis of fl/fl versus Δ/Δ MEP cells. C. Gene ontology (GO) term analysis of genes identified as downregulated by bulk RNA-seq in the *Atf4*-depleted MEP cells (versus the control group). D. Heat map showing replication of samples of ATAC-seq from fl/fl and Δ/Δ BM MEP cell samples. E. ATAC-seq profile and heat map showing the degree of chromatin accessibility around TSS ± 3 Kbp of fl/fl and Δ/Δ MEP cells. F. Venn diagram of ATAC-seq data showing the 29,493 different peak distributions of *Atf4*-deficient MEP cells. G. H3K4me3 CUT&Tag profile and heat map showing TSS ± 3 Kbp. H. Venn diagram showing the overlap between downregulated/transcriptionally repressed genes identified by ATAC-seq, H3K4me3 CUT&Tag analysis, RNA-seq after *Atf4* deletion. I. GO term analysis of the overlapping downregulated genes; only the top 11 GO terms are listed. J. qRT-PCR analysis of the indicated genes in MEP cells sorted from the fl/fl and Δ/Δ mice (n = 3 samples). K. IGV software was used to visually present the important genomic regions of *Klf1* and *Tal1* using findings from ATAC-seq and H3K4me3 CUT&Tag (shown as peaks). Data represent the mean ± SD. ***, $P < 0.001$; unpaired two-tailed Student's *t*-test.

Figure 6. ATF4 regulates ribosome biogenesis by directly activating the transcription of *Rps19bp1.*

A. Venn diagram depicting the overlapping downregulated/transcriptionally repressed genes identified from four different datasets (i.e., ATAC-seq, H3K4me3 CUT&Tag, RNA-seq, and scRNA-seq) after *Atf4* deletion. B. qRT-PCR analysis of the indicated genes in MEP cells sorted from the fl/fl and Δ/Δ mice (n = 3 samples). C. Lollipop plot displaying the top 10 predicted ATF4-targeting genes within the CMP population using pySCENIC. D. Expression of Rps19bp1 projected onto the UMAP plot of fl/fl and Δ/Δ CMP cells based on scRNA-seq data. Color intensity indicates expression levels. E. IGV software was used to visually present the important genomic regions of Rps19bp1; ATAC-seq and H3K4me3 CUT&Tag peaks, predicted cis-regulated

elements, and luciferase reporter clone region are shown. F. Schematic diagrams of the pGL3-Rps19bp1-promoter-luciferase reporter constructs (Pro-1 contains the CTCF-bound region; Pro-2 does not contain the CTCF-bound region); relative luciferase activity was determined by sequential normalization to *Renilla* luciferase and pGL3-vector activity (n = 3 samples). G. qChIP of ATF4 with primers covering the promoters of *Rps19bp1* (n = 3 samples). H. Ribosomes were separated from MEL cells transduced with control or *Atf4* shRNA-mix (shRNA-1 and shRNA-2) and then analyzed by western blotting using antibodies targeting the indicated proteins. I. Protein synthesis in hematopoietic stem and progenitor cells based on OP-Puro incorporation *in vivo* (n = 4 mice in 3 independent experiments). J. Experimental workflow showing how cKit$^+$ cells were sorted from the BM of fl/fl and Δ/Δ mice and then transduced with vector-TD or Flag-Rps19bp1-TD for the plating colony and SUnSET assays. K. TD$^+$ cKit$^+$ cells of the fl/fl and Δ/Δ mice were treated with puromycin and then analyzed by western blotting using antibodies against the indicated proteins. L. Ribosomes were separated from MEL cells transduced with control or *Atf4* shRNA-mix and vector-TD or Flag-Rps19bp1-TD then analyzed by western blotting using antibodies against the indicated proteins. M-N. BFU-E (M) or CFU-E (N) colony assays of 2×10^4 transduced TD$^+$ cKit$^+$ cells from fl/fl or Δ/Δ mice cultured in MethoCult™ SF M3436 or M3334 methylcellulose-based medium with EPO cytokine for 10 days (M) or 48 h (N), respectively (n = 3 wells in 3 independent experiments). Representative images (left), colony numbers (right) are shown. O. Experimental workflow of the transplantation assay in which 10^5 cKit$^+$ cells (sorted from the BM of the fl/fl or Δ/Δ mice and transduced with vector-TD or Flag-Rps19bp1-TD, Flag-Rps19bp1-Mut-TD) and 10^6 BM cells from donor mice (β-actin-GFP) were infected into irradiated CD45.1 recipient mice. P. Percentage of GFP$^-$Ter119$^+$ erythrocytes in the PB erythrocytes of recipient mice at the indicated time-points after the BM transplantation (n = 3-5 mice). Data represent the mean ± SD. *, $P < 0.05$; **, $P < 0.01$; ***, $P < 0.001$; unpaired two-tailed Student's *t*-test for figure 6B, 6F-G, 6I; one-way ANOVA followed by an unpaired two-tailed Student's *t*-test for Figure 6M-N, 6P.

Figure 7. 5-FU stress accelerates *Atf4*-deletion-induced BM hematopoietic failure.

A. Experimental workflow for sorting of CMP cells from the BM of fl/fl and Δ/Δ mice for ribosome profiling by Ribo-seq. B. Plots showing the differentially expressed genes identified by Ribo-seq analysis in CMP cells from fl/fl versus Δ/Δ mice. C. GSEA plot of ribosome biogenesis based on Ribo-seq data from CMP cells of the fl/fl and Δ/Δ groups. D. GSEA plot of ribosome biogenesis based on RNA-seq data from CMP cells of the fl/fl and Δ/Δ groups. E. GSEA plot of PreCFU-E based on RNA-seq data from CMP cells of the fl/fl and Δ/Δ groups (left). Relative changes in translation efficiency for the selected transcripts from the PreCFU-E gene set are shown in blue, and relative changes in mRNA expression are shown in red (right). F. Sorted cell populations from fl/fl and Δ/Δ mice were treated with puromycin and then analyzed by western blotting using antibodies against the indicated proteins. G. Representative polysome profiles from cKit$^+$ cells of fl/fl and Δ/Δ mice. Absorption profile of a linear sucrose gradient at 254 nm is depicted, with the sedimentation and major ribosomal peaks indicated. H. Survival curves of the fl/fl and Δ/Δ mice treated with a single dose of 5-FU. I. BM cell numbers of fl/fl and Δ/Δ mice 10 days after the 5-FU treatment (n = 3–4 mice). J. Number of LT-HSCs in the BM of fl/fl and Δ/Δ mice 10 days after 5-FU administration (n = 3 mice). K. The routine blood parameters of fl/fl and Δ/Δ mice at the indicated time-points after 5-FU treatment (n = 4–9 mice). L. cKit$^+$ cells from the BM of fl/fl and Δ/Δ mice were given 5-FU and then 10 days later treated with puromycin and analyzed by western blotting using antibodies against the indicated proteins. Data represent the mean ± SD. **, $P < 0.01$; ***, $P < 0.001$; unpaired two-tailed Student's *t*-test.

Figure 1

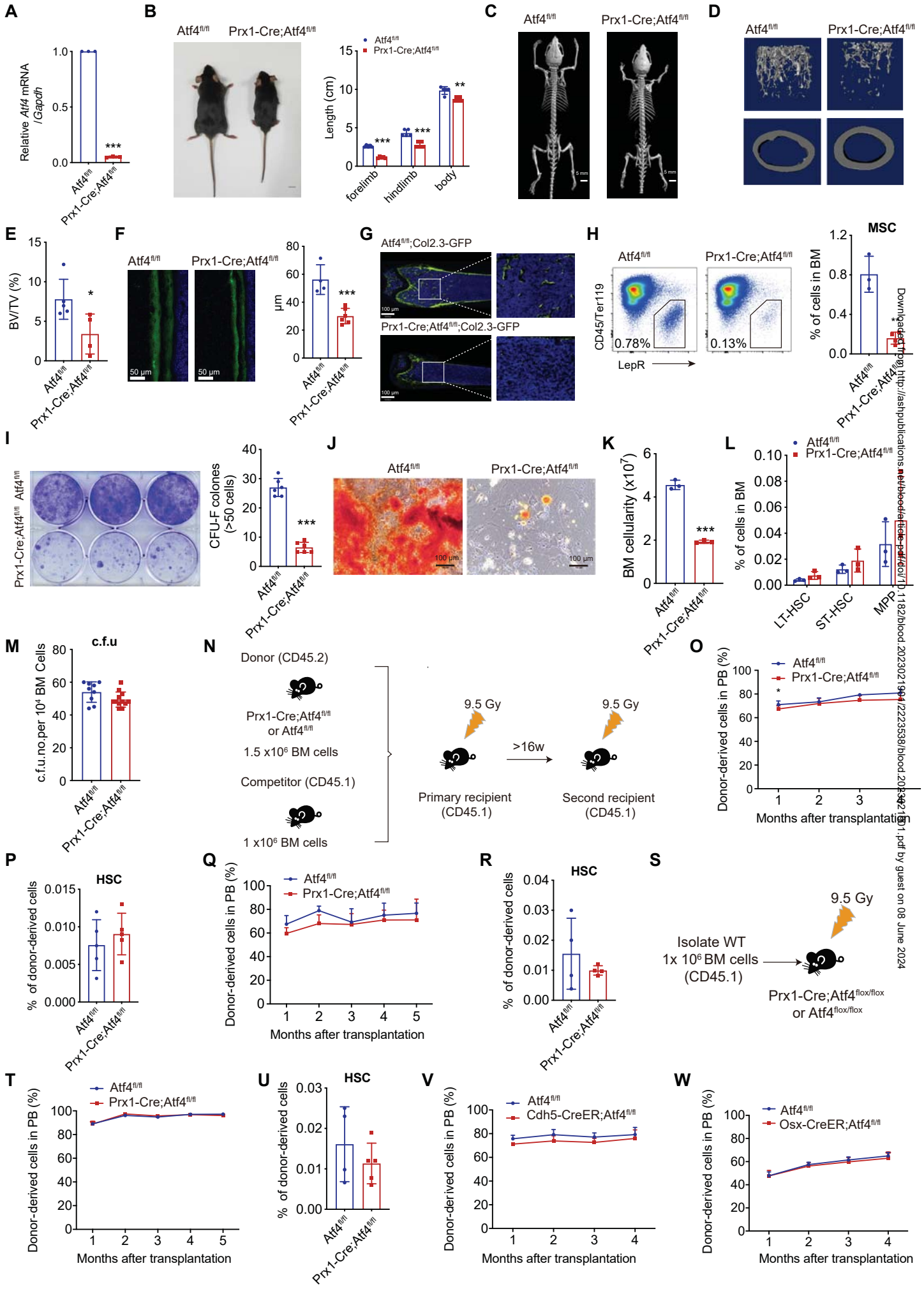

Figure 2

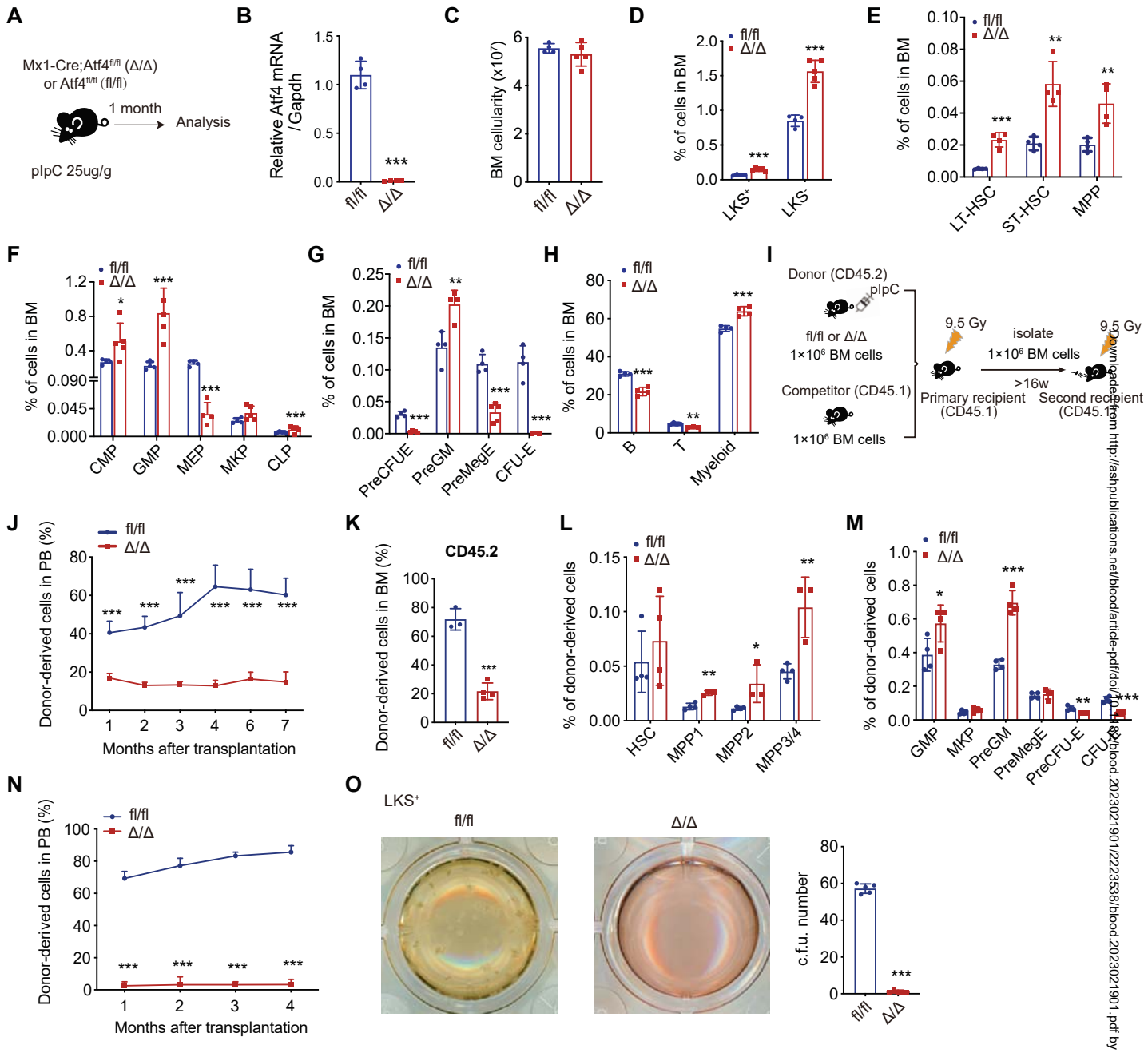

Figure 3

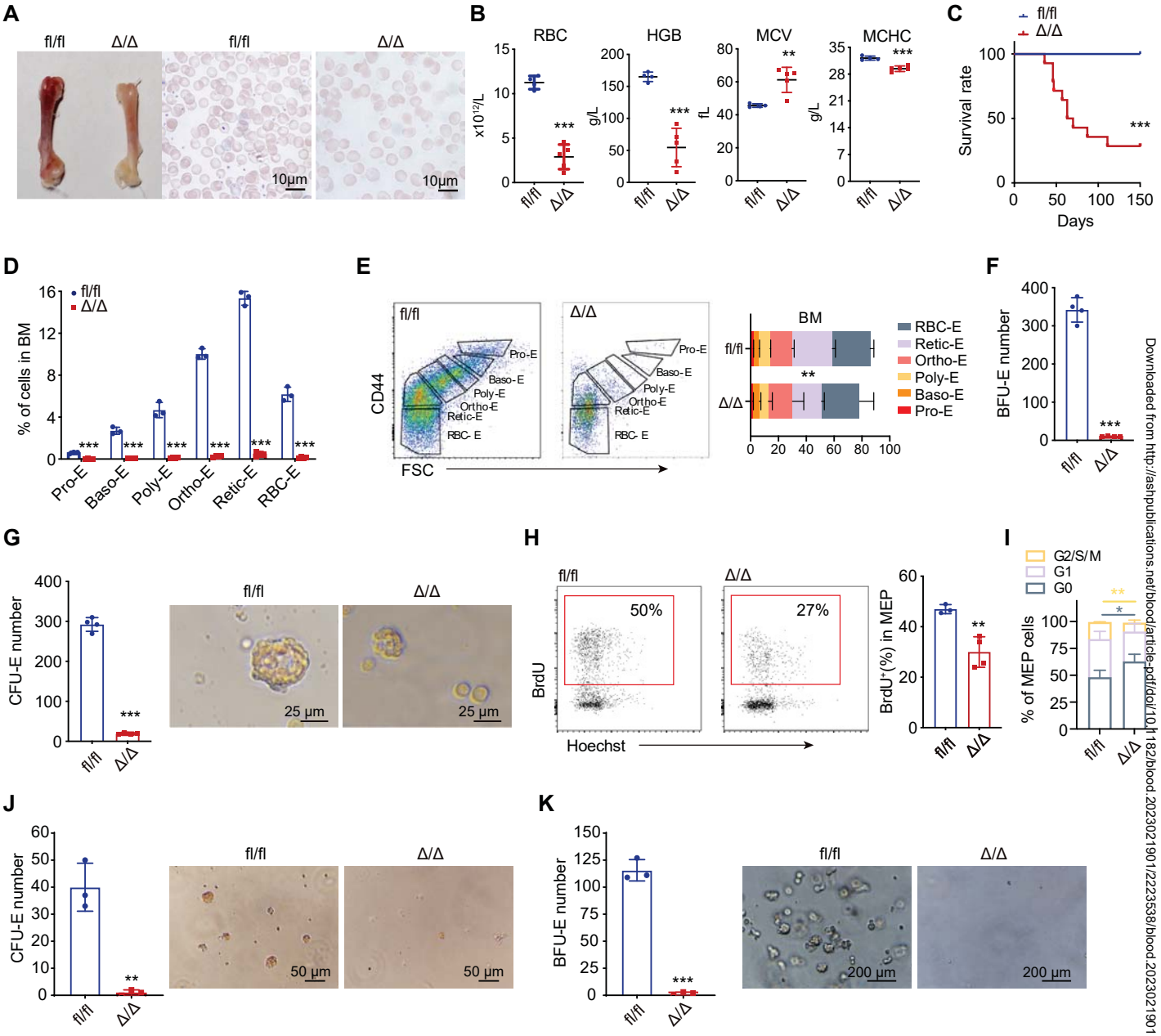

Figure 4

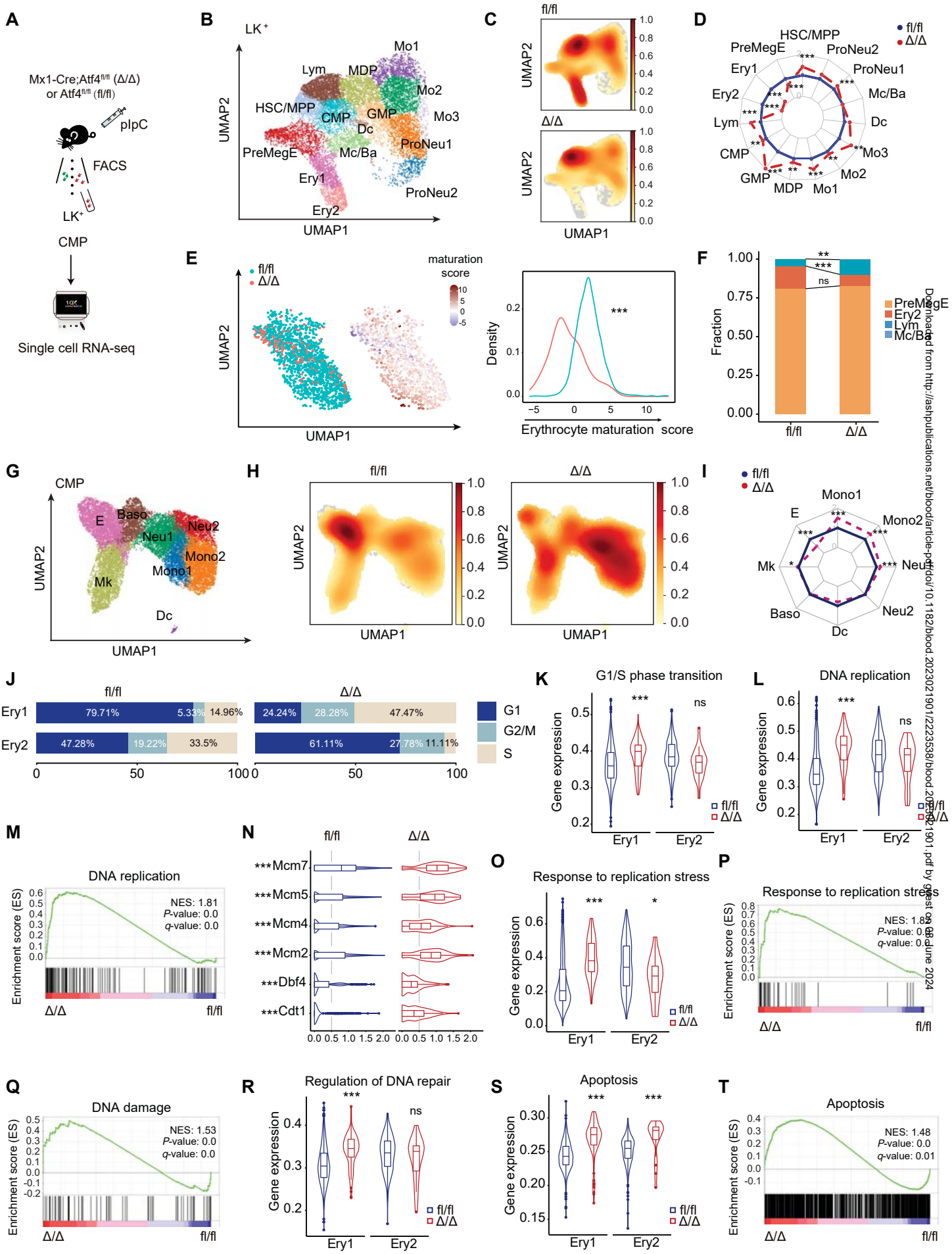

Figure 5

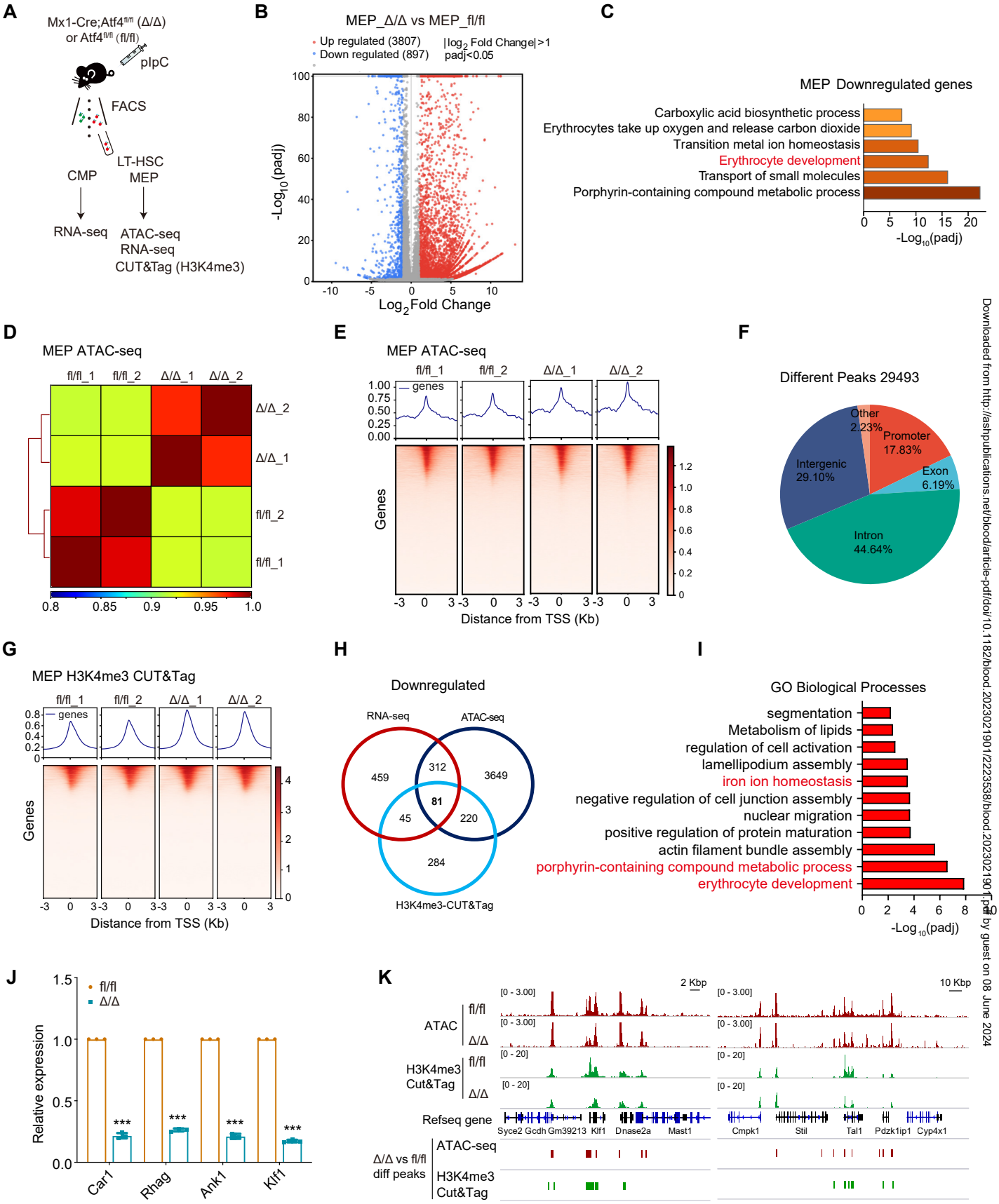

Figure 6

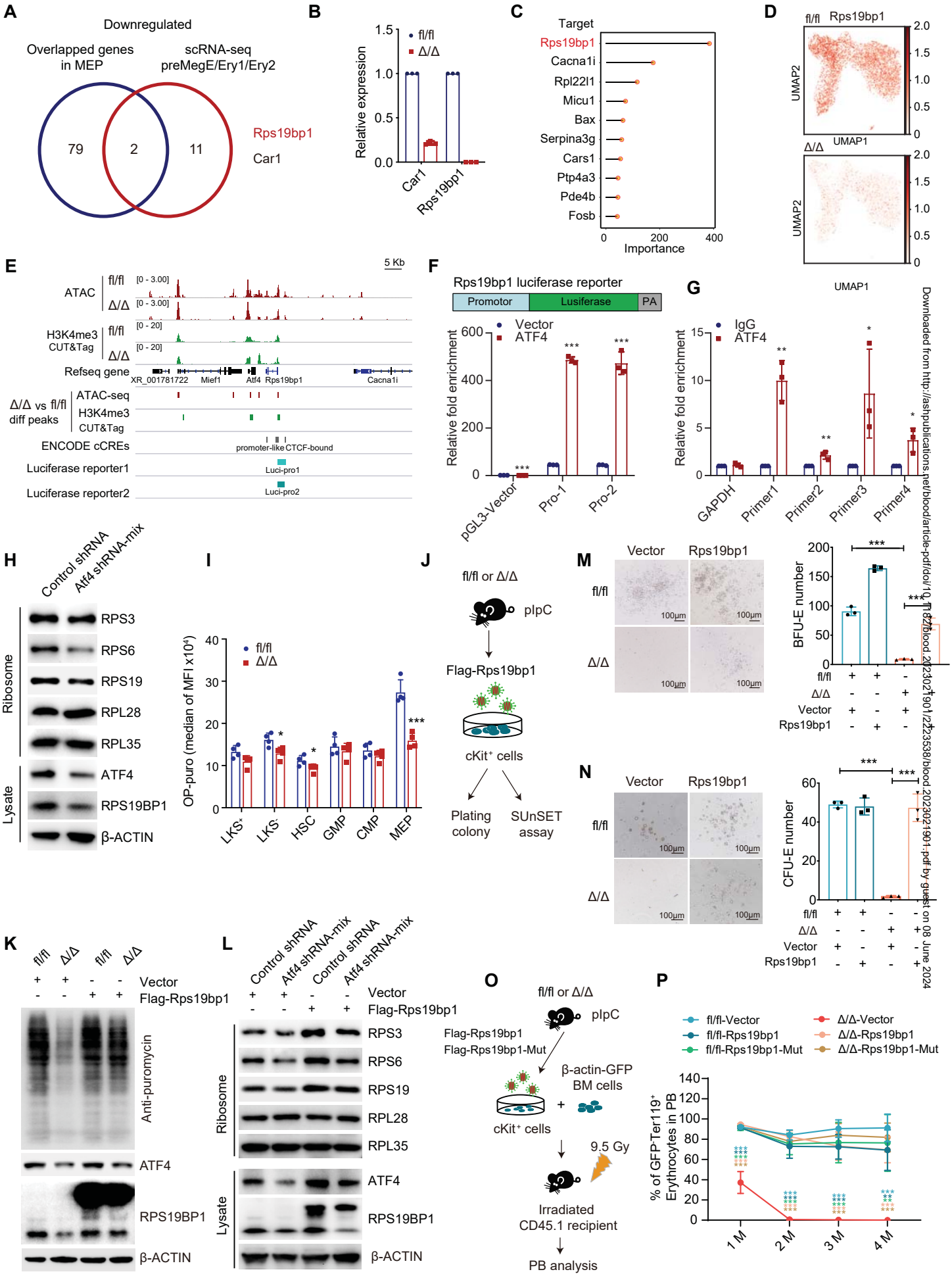

Figure 7

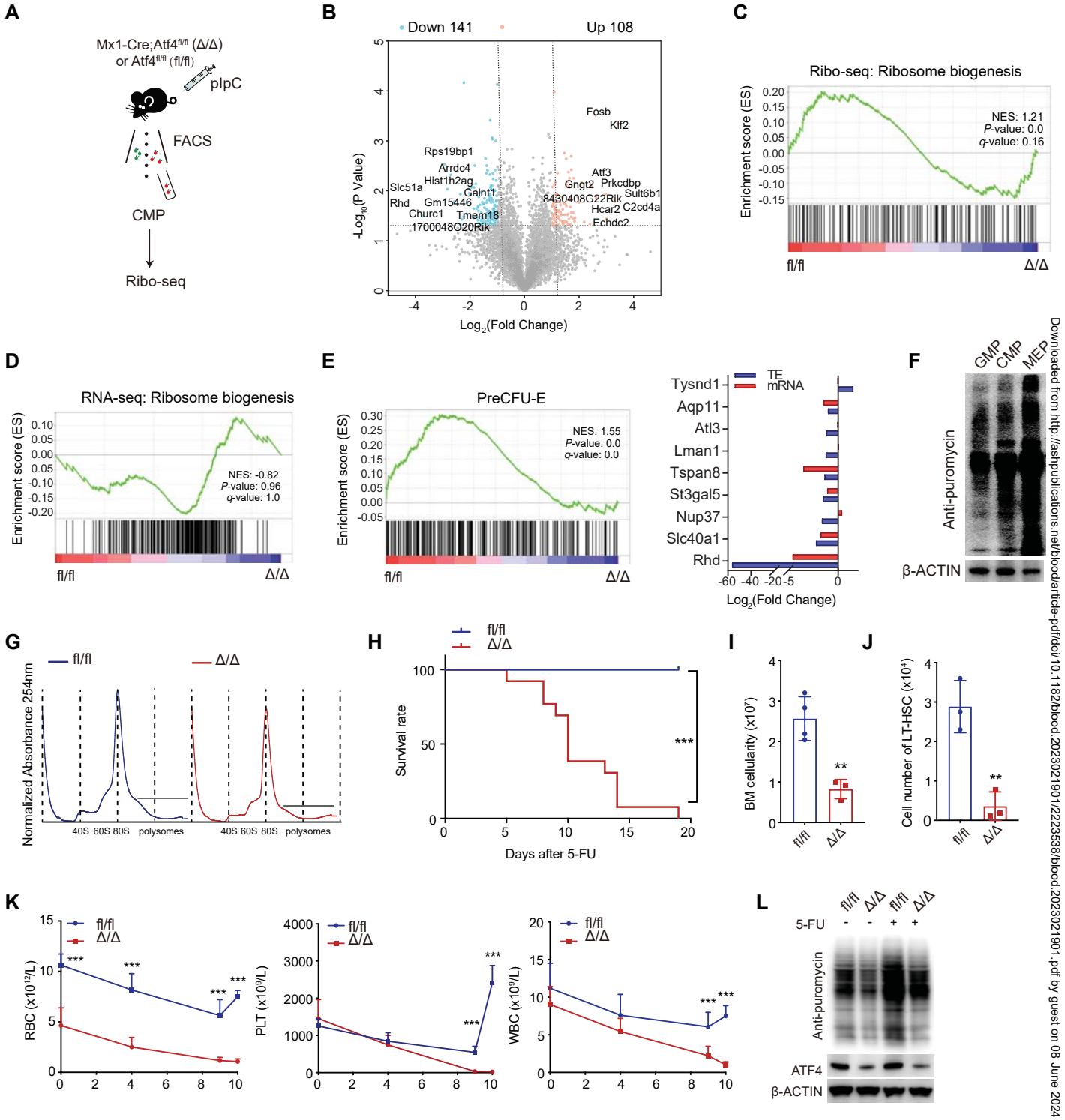

Activating Transcription Factor 4 (ATF4), Ribosome Biogenesis, and Regulation of Erythropoiesis

Megakaryocyte-erythroid progenitors (MEPs) under normal conditions

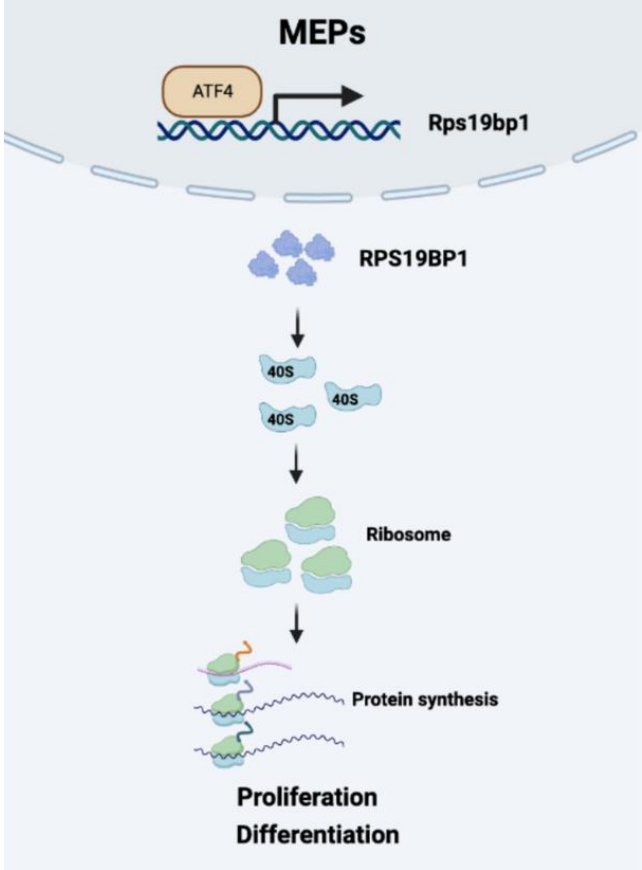

Atf4-deficient megakaryocyte-erythroid progenitors (MEPs without Atf4)

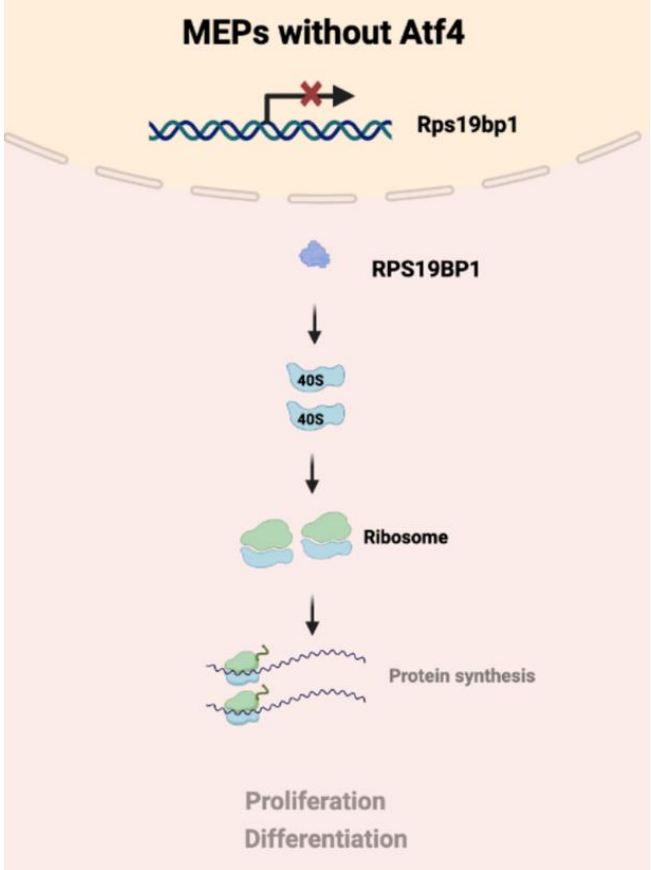

Conclusions: 1) In hematopoietic cells, ATF4 directly regulates the transcription of Rps19bp1, which in turn coordinates ribosome biogenesis promoting erythropoiesis. 2) Hematopoietic cells that are deficient in Atf4 exhibit impaired self renewal and defective erythroid differentiation.

*Zheng et al. DOI: 10.xxxx/**blood**.2024xxxxxx*

***Blood* Visual Abstract**